Flanking Fractures and the Formation of Double Ridges on Europa

Andrew J. Dombard[a,*], G. Wesley Patterson[b], Adam P. Lederer[a], and Louise M. Prockter[b]

[a]The Department of Earth and Environmental Sciences (MC-186), University of Illinois at Chicago, 845 W. Taylor St., Chicago, Illinois 60607-7059

*Corresponding Author E-mail: adombard@uic.edu

[b]The Johns Hopkins University Applied Physics Laboratory, 11100 Johns Hopkins Rd., Laurel, MD 20723

Pages: 19 (including abstract)

Figures: 7

Proposed Running Head: Flanking Fractures and Double Ridges on Europa

Editorial correspondence to:
Andrew J. Dombard
Dept. of Earth and Environmental Sciences (MC-186)
University of Illinois at Chicago
845 W. Taylor St.
Chicago, Illinois 60607-7059
Phone: 312-996-9206
Fax: 312-413-2279
Email address: adombard@uic.edu

ABSTRACT

Europa, a satellite of Jupiter, is one of the most intriguing worlds in the solar system. Its dearth of impact craters and plethora of surface morphologies point to a dynamic evolution of its icy shell in geologically recent times. Double ridges are a common landform and appear to have formed over a significant fraction of the satellite's observed geologic history. Thus, understanding their formation is critical to unraveling Europa's history, and many models have been proposed to explain their creation. A clue to the formation of ridges may lie in evidence for flexure of the lithosphere in response to a load imposed by the ridge itself (marginal troughs and subparallel flanking fractures). When this flexure has been modeled, a simple elastic lithosphere has typically been assumed; however, the generally thin lithospheres suggested by these models require very high heat flows that are inconsistent with Europa's expected thermal budget (of order 1 W m^{-2} vs. of order 10 mW m^{-2}). Each of the proposed formational models, however, predicts a thermal anomaly that may facilitate the flexure of Europa's lithosphere. Here, we simulate this flexure in the presence of these anomalies, as a means to evaluate the different models of ridge formation. We find that nearly all models of double ridge formation are inconsistent with the observation of flexure (specifically the flanking fractures), except for a cryovolcanic model in which the growing ridge is underlain by a cryomagmatic sill that locally heats and thins the lithosphere.

Key Words: Geophysics; Tectonics; Jupiter, satellites; Europa

1. Introduction

Europa, a satellite of Jupiter, is one of the most intriguing worlds in the solar system. Only slightly smaller than the Moon, Europa possesses a metallic core and a rocky mantle surrounded by a shell of water/water ice ~100 km thick (Anderson et al., 1998; Schubert et al., 2009). Its dearth of impact craters and plethora of surface morphologies point to a dynamic evolution of its icy shell in geologically recent times (e.g., Greeley et al., 2004; Schenk et al., 2004; Bierhaus et al., 2009). In addition, the preponderance of evidence points to a liquid water ocean beneath the ice shell (e.g., Pappalardo et al., 1999; Kivelson et al., 2000). Because liquid water is a necessary (but insufficient) biological requirement, Europa is one of the prime candidates for extraterrestrial life in the solar system. This ice shell is of order 10 km thick (see Schenk and Turtle, 2009), but regardless of whether the shell is somewhat thinner or thicker, the heat flow coming out of Europa is likely greater than what can be supplied by radiogenic heating in the silicate portion (see, e.g., Schubert et al., 2004; Ruiz, 2005; Sotin et al., 2009). This fact implicates tidal dissipation as the engine that drives Europa's diverse (and ongoing?) activity.

Ridges are the most ubiquitous landform on Europa, with multiple generations of ridges cross-cutting each other (for reviews, see Pappalardo et al., 1999; Greeley et al., 2004; Prockter and Patterson, 2009). These features can run remarkably uniformly for more than 1000 km across the surface, a challenge for any model of their formation. A wide spectrum of morphologies has been classified as ridges on Europa, from isolated troughs to ridge complexes that display a series of subparallel features (Head et al., 1999). The most common form is known as the double ridge (Fig. 1); these features are generally ~0.5-2 km wide, ~100-300 m tall, and possess a central trough and outer flanks with slopes typically $< 20°$ (Head et al., 1999; Coulter et al., 2009; Coulter and Kattenhorn, 2010). These shallow angles on the outer flank are usually interpreted as less than the angle of repose, suggesting non-granular processes are at work. On the other hand, materials can display a wide range of repose angles, including down to ~10°, depending on the size, shape, and stickiness of the particles (e.g., Zhou et al., 2002), as well as the gravity of the target body (Kleinhans et al., 2011). The outer flanks of double ridges appear to be dominated by mass-wasting processes. Head et al. (1999) reported that the terrain immediately peripheral to a ridge can be traced up the flank of the ridge, suggesting that the ridges represent upwarping of the pre-existing terrain. This interpretation, however, is not unique (Sullivan et al., 1998); if ridges formed by deposition of material on the surface, they would reflect to some degree the topography of the underlying terrain. Furthermore, some of the cracks that persist up the flanks could be due to reactivation along pre-existing structures. A subtle marginal trough a few tens of meters deep is fairly common (see Hurford et al., 2005), and subparallel, presumably tensile fractures can sometimes be found near the outer reaches of these troughs (Fig. 1). Additionally, the marginal troughs can sometimes possess diffuse regions of lower albedo, suggesting burial or processing of the terrain.

Several models have been proposed for the formation of double ridges (to be reviewed in the next section). All of these models appeal to exploitation of a pre-existing crack in the ice shell of Europa. Addressing the source of the initial crack has been beyond the scope of these models (and continues to be so in this current work), but it is thought that the cracks form in response to externally applied stresses (Greeley et al., 2004; Kattenhorn and Hurford, 2009). As pointed out by Greeley et al. (2004), "each model has different implications for the presence and distribution of liquid water at the time of ridge formation." Given that ridges are the most ubiquitous landform, it is therefore critical to understand ridge formation in order to decipher Europa's unique history.

A clue to the formation of ridges may be provided by evidence for flexure of the lithosphere in response to a load imposed by the ridge itself. Several groups have interpreted the presence of marginal troughs and subparallel flanking fractures associated with ridges as characteristic of flexure (e.g., Pappalardo and Coon, 1996; Tufts, 1998; Billings and Kattenhorn, 2005; Hurford et al., 2005; Dombard et al., 2007). The addition of a ridge to the surface will cause the lithosphere to warp downward, producing marginal troughs and uplifting a flexural bulge peripheral to these troughs that may be detectible. Between the bulge and the trough, tensile flexural stresses peak and may produce subparallel fractures (arrows in Fig. 1). When this flexure is modeled, a simple elastic lithosphere has usually been assumed (see Turcotte and Schubert, 2002); however as we will discover below, the generally thin lithospheres indicate very high heat flows inconsistent with Europa's expected thermal budget, which implicates a localized thermal anomaly in the formation of the double ridges (cf. Dombard et al., 2007).

In this paper, we will evaluate models of double ridge formation by determining which ones are consistent with the observation of flexure. As we will discuss, ridges that display evidence of flexure (marginal bulges, troughs, and fractures) are common but not abundant, and those that possess evidence of flexure can provide important constraints. Because the bulge and trough topography is subtle, we will specifically look to see which models, and under what conditions, predict tensile stresses that peak at the right range of distances away from the central ridge axis, and thereby are able to reproduce the flanking fractures. In the next section, we review the various models that have been proposed and discuss the thermal anomalies that may be associated with each one. Then, we discuss a suite of measurements of double ridges, in order to determine the range of distances of the flanking fractures. We subsequently describe our thermal-mechanical finite element simulations, present our results, and discuss the implications.

2. Models of Double Ridge Formation

Many of the proposed models for double ridge formation are summarized in Fig. 2. In the volcanic model of Kadel et al. (1998), a pre-existing crack provides a pathway for fissure eruptions that build the ridges cryoclastically (Fig. 2a). In the tidal squeezing model of Greenberg et al. (1998), daily tidal forces cause the crack to open and close, squeezing material onto the surface (Fig. 2b). A dike intrusion model (Turtle et al., 1998) posits that injection of melt into the subsurface can deform the lithosphere around the crack, uplifting the ridge. An ice wedging model (Melosh and Turtle, 2004; Han and Melosh, 2010) represents a hybrid between the tidal squeezing and dike intrusion models. Here, water fills a crack that opens during the tensile part of a tidal cycle but does not reach the surface because of enhanced cooling; the subsurface build-up of ice wedges open the crack and deforms the surface, producing the ridge. Head et al. (1999) proposed that the crack leads to formation of a wall diapir of warm ice that uplifts the ridge (Fig. 2c), while Sullivan et al. (1998) argued that the ridge represents a symmetric buckle of the lithosphere adjacent to the crack under a compressive stress state (Fig. 2d). A shear heating model (Gaidos and Nimmo, 2000; Nimmo and Gaidos, 2002; Han and Showman, 2008) has been proposed where cyclical strike-slip motion on a crack dissipates heat in the interior, resulting in the warmer, buoyant ice uplifting the ridge (Fig. 2e).

Last, Dombard et al. (2007) recently proposed a variant of the cryovolcanic model. In volcanic systems on Earth, the amount of subsurface magmatism generally exceeds the amount of surface volcanism, often by a large amount (Crisp et al., 1984). On an icy satellite, it is reasonable to expect this phenomenon to hold, especially since the cryomagma (water) is denser than the country rock (ice). Thus, we have proposed that while the ridge is being built on the surface effectively as a cryoclastic fissure eruption (Kadel et al., 1998), a cryomagmatic sill forms at a depth of ~1 km, at the level of neutral buoyancy of water in an ice shell (Fig. 3).

For the purposes of this work, these models may be assigned to different classes. Some of these models are not consistent with the presence of the flanking fractures. The dike intrusion model (Turtle et al., 1998), ice wedging model (Melosh and Turtle, 2004; Han and Melosh, 2010), and the compression model (Sullivan et al., 1998) predict local to regional compressive stresses immediately exterior to the ridge, which would inhibit the formation of the fractures; thus, we will not consider these models further. The cryovolcanic model of Kadel et al. (1998) and the tidal squeezing model (Greenberg et al., 1998) have liquid water arising solely along the pre-existing crack; we classify these mechanisms as “central conduit” models. Our cryovolcanic sill variant (cf. Dombard et al., 2007) adds the thermal effects of a sill to the central conduit models (Fig. 3). The wall diapir model (Head et al., 1999) is like the shear heating model (Gaidos and Nimmo, 2000; Nimmo and Gaidos, 2002; Han and Showman, 2008) in that the buoyancy that raises the ridge comes from thermal expansion due to heating along a vertical plane in the ductile substrate that underlies the pre-existing crack in the brittle surface layer; thus we will consider these as one class that we will call “ductile heating.”

Consequently, we will consider 3 classes: central conduit, cyrovolcanic sill, and ductile heating. Each class predicts a distinct thermal structure near the growing ridge, with a thermal anomaly overprinted on a background state. The flexure that we seek to simulate occurs in the lithosphere, which is the mechanical surface layer that can support stresses over geologic time. This layer is not pliable over tidal time scales, so any bulk tidal dissipation will occur deeper in the ice shell. Thus, the background thermal state is simply the conductive passage of heat generated within the interior of Europa (via tidal dissipation and decay of long-lived radioactive nuclides in the silicate interior), with an expected surface heat flux in the range of several tens of mW m^{-2} (see Schubert et al., 2004; Sotin et al., 2009). In the central conduit class, the pre-existing crack is filled with water very near its freezing point, and these temperatures will diffuse into the surrounding ice. In addition to a central conduit thermal anomaly, the cryovolcanic sill model proposes injection of a horizontal sheet of water near its freezing point, resulting in a wider thermal anomaly than the central conduit models (Fig. 3). Last, the ductile heating models predict localized heating in the ductile portion of the ice shell, strongest in the plane underneath the pre-existing crack and decreasing with horizontal distance, resulting in a thermal anomaly also wider than the central conduit models. We take the temperature field predicted in Nimmo and Gaidos (2002) to be representative of this process.

3. Measurements of Double Ridges

Following Billings and Kattenhorn (2005), we compare the predicted lateral distance to peak tensile flexural stresses from our simulations to the distances to fractures parallel to double ridges. Thus, important constraints for our method are the distance to flanking fractures and the half-width of the ridge. Billings and Kattenhorn (2005) identified flanking fractures associated with 3 ridges on Europa: Androgeous Linea, Ridge C2r (Tufts et al., 1999), and Ridge R (Tufts et al., 1999). Billings and Kattenhorn (2005) measured distances to fractures at 2-5 randomly spaced locations along each ridge; in contrast, we measure ridge widths and the distance to fractures at locations spaced 1 to 2 km apart along each ridge (20 measurements for ridge R and 30 for Androgeous Linea and Ridge C2r), determining an average value and a standard deviation. All measurements were obtained from geo-referenced Galileo images. We have examined all Galileo images with sufficient resolution to reveal these relatively fine scale fractures, finding examples that flank a ridge in a region pervasively covered by multiple generations of ridges (cf. Billings and Kattenhorn, 2005; Hurford et al., 2005). Thus, ridges with evidence of fracture are common but not abundant. Apart from the evidence of flexure, these ridges are morphologically similar to the other ridges in the image, which argues against them having formed from a different mechanism.

For Androgeous Linea, we find an average ridge half-width of 1.00 ± 0.11 km (one standard deviation) and an average distance to fractures of 2.85 ± 0.17 km. For Ridge C2r, these distances are 1.98 ± 0.23 km and 2.90 ± 0.25 km, and for Ridge R, they are 0.62 ± 0.07 km and 1.40 ± 0.19 km. Our measurements are comparable to past work. As demonstrated by the relatively small standard deviations, the lateral distances to the flanking fractures remain fairly constant over long distances for an individual ridge; however, there is significant variability among ridges. Thus, we consider a lateral distance to the flanking fractures of 2 km but recognize that any mechanism must explain distances between ~1 and ~3 km.

4. Finite Element Simulations

Our goal is to test which classes of formational models detailed in Section 2 are consistent with observation of lithospheric flexure determined in Section 3. Specifically, we will examine situations that are most favorable to flexure, in order to rule out those classes of models that cannot result in any observable flexure for all reasonable situations. To investigate the deformation of the lithosphere in the presence of these thermal anomalies, we use the commercially available MSC.Marc finite element package, which we have used many times to study the geodynamics of icy satellites (e.g., Dombard and McKinnon, 2000, 2006a, b; Dombard et al., 2007; Kay and Dombard, 2011; Damptz and Dombard, 2011). We simulate a plane-strain system, 5 km deep and 10 km wide, subdivided into 5000 quadrilateral elements (100 evenly spaced elements horizontally and 50 elements vertically, with a bias to concentrate more elements near the surface). The dimensions of the space and the resolution of the mesh are designed to impact negligibly the quality of our results (though we will discuss certain situations where the distance to the far side boundary may be an influence). The left side of the simulated space is assumed to be the central axis of the ridge system, so all boundary conditions there enforce symmetry. The process first involves a simulation of the thermal state, the results of which are imported into a mechanical simulation.

For the thermal simulation, we use the thermal conductivity of water ice of Klinger (1980), which is inversely proportional to temperature. This conductivity is ~15% smaller than a later version with the same functional form by Petrenko and Whitworth (1999), which is a simplified fit to data from the same era as Klinger (circa 1980); however, lower conductivity translates into higher thermal gradients for a given heat flux, which achieves our goal of testing conditions most favorable to flexure. The surface temperature is locked at a constant value, usually 100 K (e.g., Moore et al., 2009). The vertical sides of our finite element mesh are constrained to zero heat flux, while a prescribed heat flux is applied to the bottom boundary. (Again, we assume any bulk tidal dissipation occurs below the lithosphere.) Models of the thermal state of the ice shell of Europa usually predict a surface heat flux of a few tens of mW m^{-2} (e.g., Schubert et al., 2004; Sotin et al., 2009); to create conditions most favorable to flexure, we usually implement a background heat flux at the higher end of this range of 40 mW m^{-2}.

The thermal anomalies are implemented by constraining the temperatures of the nodes (the corners of the quadrilateral elements) at the proper positions. For instance, simulation of the central conduit model involves constraining the nodes on the central axis to 270 K. The central axis nodes are also constrained for the sill model to 270 K, as well as a line of nodes 1 km deep out to a prescribed distance away from the central axis. For the ductile heating model, we digitize the anomalous temperature from Fig. 2d of Nimmo and Gaidos (2002), adding these values to our background heat flow state. We then determine the steady-state solution to all these conditions. We elect to investigate an equilibrium solution, as opposed to a transient solution in which the domain heats or cools in response to application of the thermal anomalies, because the steady-state solution will create the warmest conditions most favorable to flexure.

These thermal solutions are then input as an initial state into our mechanical simulations. The rheology has 3 components: elastic (which ultimately provides the strength of the lithosphere), viscous (to simulate temperature- and time-dependent ductile creep in ice), and plastic (a continuum approximation of discrete brittle faulting). A direct consequence of this multicomponent rheology is that the thickness of the lithosphere does not need to be input a priori, but instead develops in response to the mechanical and thermal state of the system; in addition, the adopted rheology also allows the lithosphere to evolve with time (see, e.g., Damptz and Dombard, 2011). We assume the rheological properties of water ice, including the elastic Young's modulus and Poisson's ratio from Gammon et al. (1983). For the ductile creep, we employ a composite flow law that incorporates a dislocation creep mechanism and a grain-boundary diffusion creep mechanism acting in series with a grain-boundary sliding (GBS) mechanism and a basal-slip mechanism that interact in a rate limiting sense (Goldsby and Kohlstedt, 2001). Both the diffusion creep and GBS mechanisms are sensitive to the ice grain size; following Dombard and McKinnon (2006a) who appealed to the analogy of terrestrial glacial ice, we consider a range of grain sizes of 0.1-10 mm, with a nominal size of 1 mm. For the plastic component, we use the results from ice friction experiments by Beeman et al. (1988).

A free-slip boundary condition is applied along the far side of the domain. Free-slip is also applied along the central (symmetry) axis of the ridge; while we could have adopted a "broken plate" condition (see Turcotte and Schubert, 2002) due to the presence of the pre-existing crack through the ice shell, mass continuity within the subsurface of Europa would enforce free-slip conditions (i.e., no lateral displacements) under the central axis. We apply a Winkler-type, buoyant restoring force on the bottom boundary. Coupled with an assumed mass density of 950 kg m^{-3}, gravity with an acceleration of 1.35 m s^{-2} is applied as a body force; because the simulated material is compressible (i.e., elastic Poisson's ratio < 0.5), the application of gravity requires the initial stress state be adjusted to lithostatic (vertical and horizontal stresses equal and growing linearly with depth). The load imposed by the ridge is simulated as a series of elemental surface pressures that step-wise approximate a 1.6 km wide (800 m half-width) and 240 m tall symmetric ridge with a triangular cross-section. We linearly increase the magnitude of these surface pressures, to approximate the growth of the ridge by deposition of material over a finite time. Because double ridges are the most ubiquitous landform on Europa, we assume a growth time of 100 kyr (enough for of order 100-1000 generations of ridges on Europa). A simulation with the load instantly emplaced (zero growth time) produced negligibly different results, demonstrating that the final deformation is insensitive to the growth time.

Although relative displacements and rotations are small (i.e., small strain conditions), we implement a full large strain formalism, because it implicitly includes buoyant restoring forces that arise from the displacement of density interfaces such as at the surface (cf. Turcotte and Schubert, 2002). Additionally, a formalism is used that enforces constant dilatation across each element, which prevents numerical errors that can arise in the simulation of nearly incompressible behavior (e.g., ductile creep). Time stepping is automatically controlled to limit everywhere in the mesh the creep strain increment to less than a quarter the elastic strain; this algorithm effectively resolves the minimum viscoelastic Maxwell time by a factor of 4. To keep the run times reasonable (~10 hr per simulation), we implement a minimum viscosity in the mesh of 10^{19} Pa s (minimum Maxwell time of 90 yr), a value generally realized below the lithosphere. Aspects of our results are sensitive to this artificial viscosity cut-off (e.g., time over which flexure develops), but our main metric for simulation success (lateral distance to peak plastic strain) is insensitive. Our measurements of double ridges show that the flanking fractures form at a distance of 2 ± 1 km away from the central axis of the ridge. Thus, the primary metric that we use to determine success or failure of our simulations is the horizontal distance on the surface at which the lateral plastic strain peaks. We have confirmed that this peak is the principal tensile strain, consistent with the formation of a flanking fracture, and we have confirmed that this position is insensitive to the choice of the viscosity cut-off. The simulations are run past the growth time (100 kyr) to 1 Myr, a time frame over which any thermal anomaly may still be extant. All results are shown at this end time of 1 Myr.

5. Results

Most studies of ridge flexure on Europa do not appeal to local thermal anomalies but implicitly assume a high regional heat flow (e.g., Billings and Katternhorn, 2005; Hurford et al., 2005). Thus, our first step is to determine the extent of lithospheric flexure under a uniform background heat flow (no anomalies), in order to ascertain the magnitude that would be necessary to produce the observed flanking fractures. A simulation with just a background heat flow of 40 mW m^{-2} resulted in no appreciable flexure; the surface was deflected by only ~10 cm, and the resulting stresses were insufficient to produce any plastic failure. The regional heat flow would need to be significantly higher (more than an order of magnitude) to be consistent with the observed fractures. Figure 4 shows the lateral distance to the peak plastic strain as a function of the background heat flow value. Io-like heat flows are required. To put the flanking fractures at

3 km, a heat flow of ~700 mW m^{-2} is needed (cf. Dombard et al., 2007). A heat flow of ~1-1.1 W m^{-2} is needed for fractures at a distance of 2 km. The curve in Fig. 4 is well fit by a function inversely proportional to the heat flow; for a lateral distance of 1 km, a heat flow > 2 W m^{-2} is needed. Figure 5 shows, for a heat flow of 1 W m^{-2}, a profile of the surface deflection and a profile of the in-plane surface plastic strain (positive values indicate extension). The contractional plastic strain near the axis would be underneath the ridge. The crest of the flexural bulge (the subtle topographic high on the periphery of the central flexural trough) is at a lateral distance of ~2.4 times the distance to the peak plastic strain. This finding suggests that for the simulations near the lower end of the heat flow range in Fig. 4 (i.e., those with distances to peak plastic strains of ~3 km or greater and thus bulge crests of at least 7-8 km distance), the far boundary at 10 km distance may be interfering with the deformation, making the values in the figure more suspect. However for a simulation with the mesh extended out to 20 km with a heat flow of 563 mW m^{-2} (i.e., the case in Fig. 4 potentially most affected by this issue), the position of peak plastic strain differs by < 3% (3.8 km vs. 3.7 km for the case with the far boundary at 10 km). Figure 5 also shows the deflection of an elastic plate under a line load (Section 3-16 in Turcotte and Schubert, 2002), where the flexural bulge crests at the same distance from the central axis as in our simulation (~5.1 km) and the magnitude is scaled to match the depth on the central axis. Using our material and planetary parameters, this elastic plate is ~140 m thick (cf. Hurford et al., 2005). Maximum bending stresses (and hence the likely position of any brittle failure) for this elastic plate occur at ~2.6 km from the central axis, slightly farther than in our simulation. Differences are due to the different rheological models and to the fact that we implement a distributed surface load.

Factors that enhance ductile creep allow for somewhat lower heat flow values. For a fracture distance of 2 km (our typical value), the requisite heat flow in a simulation with a higher surface temperature of 110 K (the average surface temperature at the equator is 106 K [Moore et al., 2009], compared to the 100 K we generally use) is lowered to closer to 800 mW m^{-2} (see Fig. 4). For a simulation with a higher surface temperature and a grain size at the small end of our considered range (0.1 mm), a heat flow of between 600 and 700 mW m^{-2} is required. Even with these enhancements, the regional heat flows needed to explain the flanking fractures are more than an order of magnitude greater than the regional heat flows expected on Europa (see Schubert et al., 2004; Sotin et al., 2009). Even estimates of maximum tidal dissipation in Europa yield maximum heat fluxes of 300-400 mW m^{-2} (O'Brien et al., 2002; Hussmann and Spohn, 2004), far less than the values we predict here. This finding implicates a thermal anomaly in the creation of the observed flexure.

The first class of thermal anomaly that we consider is the ductile heating model. The application of the thermal anomaly from Nimmo and Gaidos (2002) on top of a background heat flow of 40 mW m^{-2} results in almost as little flexure as the case with no anomaly (~30 cm vs. ~10 cm of surface deflection, with no plastic strain). The anomaly digitized from Nimmo and Gaidos (2002) used a brittle-ductile transition of 2 km depth; one might expect that a shallower transition would squeeze the isotherms, producing a higher localized heat flow and more flexure. When we cut the vertical (and horizontal) extent of the anomaly in half while keeping the same excess temperatures however, the flexure is a bit less (~25 cm) because of the reduced horizontal extent of the anomaly. Even cases that account for factors that enhance ductile creep (higher surface temperature and smaller grain size) see negligible flexure (at most an increase in surface deflection of ~2.5 times and still no plastic strains).

Simulations testing central conduit models do result in plastic strain at the surface; however, the failure is located very close to the central axis (within ~100 m, so therefore under the ridge itself), where the thermal anomaly weakens the lithosphere the most. The plastic strain is also negative, indicating contractional failure in a zone where the surface of the down-flexed lithosphere is squeezed. Total vertical deformation is limited to ~2 m. Enhancing ductile creep with a higher surface temperature and a smaller ice grain size results in ~21 m of total vertical deformation; however, the displacements are concentrated near the central axis. At 800 m from the axis (i.e., the edge of the ridge), the total displacement is < 7 m. The ductile-creep enhanced case does experience a zone of extensional plastic failure, but it peaks at 600 m from the axis (again, under the ridge itself). Like the ductile heating class, the central conduit class does not result in deformation consistent with the flexure observed at double ridges. Even though peak excess temperatures are higher and closer to the surface than in the ductile heating class, the lateral extent of the thermal anomaly is too small to affect enough of the lithosphere. This finding motivates a ridge formation model with a wider thermal anomaly.

Such widening is accomplished if a cryovolcanic sill is simulated by constraining the temperature to 270 K of the nodes ~1 km deep to a certain distance away from the central axis. This constraint produces a thermal anomaly, more laterally extended than the other classes, with a localized surface heat flow of 563 mW m^{-2}. The behavior of the system is more complex, however, than simply considering a situation with a background heat flow of that value (see Fig. 4) or even a central conduit model with a background heat flow of 563 mW m^{-2}. The localized thermal anomaly results in a relatively thin, weak lithosphere above the sill, transitioning into a thick, very strong lithosphere at lateral distances beyond the sill. This squeezes the deformation into a smaller zone. The resultant plastic failure of the surface then depends on the lateral extent of the sill (Fig. 6). For narrow sills, the peak plastic strain occurs near the edge of the sill, in the transition zone from thin to thick lithosphere at the edge of the thermal anomaly; however for sills wider than ~4 km from the central axis, peak plastic strains occur inward from this transition zone.

This change indicates 2 different behavioral regimes, which are shown in Fig. 7. The edge of a sill with a half-width of 8 km is very near the lateral position of the crest of the flexural bulge for the case of simply a high regional heat flow of 563 mW m^{-2} (at ~9.2 km). Thus, the deformation associated with the localized thermal anomaly is squeezed into a smaller area than it would be without the anomaly, concentrating the stresses and producing a general zone of plastic failure over the entire anomaly. The deformation is not so squeezed, however, such that there are still peak bending stresses (and hence plastic failure) at some point within this zone. For a much more narrow anomaly, the deformation is squeezed into such a narrow zone that stresses are strongly concentrated right at the transition from thin to thick lithosphere. Between ~4 km and ~5 km, there is a transition between these regimes.

In addition, the distance to the peak plastic strain is insensitive to differences in various parameters. Simulations with smaller regional heat flows, different (higher and lower) surface temperatures, and different (smaller and bigger) ice grain sizes still have peaks at the same distances as shown in Fig. 6. A somewhat counterintuitive result, this insensitivity arises because the system is less dependent on the thickness of the lithosphere and more dependent on the squeezing of the deformation into a narrower lateral zone.

6. Discussion and Conclusion

The central motivation of this work is to evaluate the models that have been proposed for the formation of double ridges on Europa on the basis of the observation of lithospheric flexure. Our results indicate that nearly every model of ridge formation is inconsistent with the observed flexure. If a ridge forms during an episode of very elevated, Io-like heat flow, the lithosphere can flex appropriately, but given how ubiquitous ridges are on Europa, this elevated heat flow state would have to be the norm. Consequently, it is likely that the flexure arises due to a locally thin lithosphere that results from a thermal anomaly. The ductile heating model does not appear to be consistent with the observation of flexure at double ridges on Europa, because the magnitude of the anomaly and the spatial extent are too limited to affect sufficiently the thickness of the lithosphere to permit the flexure. In fact, the situation is even more dire than our results indicate, because a component of the ductile heating models (e.g., Head et al, 1999; Nimmo and Gaidos, 2002) is that the ridge itself comes from the buoyancy of the thermal anomaly, necessitating that the lithosphere deform on a horizontal scale of the width of the ridge (kilometer scale), while our simulations show the lithosphere deforming on a much wider scale (> 10 km). A variant of the shear heating model, developed to explain the plumes of icy particles emanating from the south polar region of Enceladus (Nimmo et al., 2007), might be adapted to explain the actual formation of a ridge as a surface build-up of erupted ice (a cryo-cinder pile), thereby bypassing the requirement that the lithosphere deform on the scale of the width of the ridge, but the thermal anomaly will still be too limited to explain the flexure. Similarly, the central conduit models yield too narrow a thermal anomaly to explain the flexure. Furthermore while models that propose regional compression are not seemingly consistent with the interpretation that the flanking fractures are extensional in nature, we can gain insight from our simulations. If anything, these models possess no anomaly or can be ascribed to the central conduit class, which yields deformation (both elevation and horizontal scale) inconsistent with double ridges.

Our simulations suggest that the injection of a cryovolcanic sill can produce a thermal anomaly and a locally thin lithosphere that is consistent with the observation of flanking fractures running parallel to double ridges. Indeed, the presence of intrusive cryomagmatism on icy satellites is logical, because the magma is denser than the country rock and will reach a level of neutral buoyancy before reaching the surface. Other researchers have also recognized this possibility for Europa, speculating on the presence of sills ~1 km deep (Collins et al., 2000; Manga and Wang, 2007). For a distance of 2 km from the central axis to the flanking fractures, our results demonstrate the best match when the sill extends ~2.3 km from the central axis. Emplacement of a sill would produce surface inflation comparable to the thickness of the sill over a horizontal scale of 1-10 km (the width of the sill); however, surface deflections of this magnitude may be difficult to observe, given currently available topographic data for Europa (e.g., Schenk, 2009). Europa has abundant topography at an amplitude of order 10 m, so while a sill of order 100 m thick should yield observable surface inflation, a thinner sill (of order 10 m) over such a long horizontal baseline would be largely invisible at present. On the other hand, our simulations also show that the distance to the flanking fractures depends on the horizontal extent of the sill. On a single ridge, the distance to the fractures does not vary significantly over the tens of kilometers they are observed, and it is a challenge to envision a scenario in which the sill maintains such a uniform width over such a long track. Furthermore, simple scaling of the solidification of a sill (see Section 4-19 in Turcotte and Schubert, 2002) indicates a 10 m thick sill will freeze in a matter of decades (using the ice parameters in Kirk and Stevenson, 1987). This is too short a time (and too little excess heat) to affect strongly the overlying isotherms, unless the central cryovolcanic conduit that feeds the growing ridge also replenishes hot water to the sill. On the other hand, these issues might explain why ridges with evidence of flexure are not abundant, because while it appears impossible to produce a ridge with the observed flexure using other formational mechanisms, it may be straightforward to produce a ridge with this sill model that lacks the observed flexure, depending on the local conditions. While the uniformity of double ridges over long distances and the relatively short timescales for freezing of a sill remain issues, our results indicate that only the cryovolcanic sill model is consistent with the observed flexure.

Acknowledgements

We thank Steven A. Hauck, II for his assistance, as well as 2 anonymous reviewers who helped us refine our arguments and improve our presentation. This research was support by NASA Grant NNX09AP28G to AJD.

References

Anderson, J.D., Schubert, G., Jacobson, R.A., Lau, E.L., Moore, W.B., Sjogren, W.L., 1998. Europa's differentiated internal structure: Inferences from four Galileo encounters. Science 281, 2019-2022.

Aydin, A., 2006. Failure modes of the lineaments on Jupiter's moon, Europa: Implications for the evolution of its icy crust. J. Struct. Geol. 28, 2222-2236.

Beeman, M., Durham, W.B., Kirby, S.H., 1988. Friction of ice. J. Geophys. Res. 93, 7625-7633.

Bierhaus, E.B., Zahnle, K., Chapman, C.R., 2009. Europa's crater distributions and surface ages. In: Pappalardo, R.T., McKinnon, W.B., Khurana, K.K. (Eds.), Europa, Univ. of Arizona Press, Tucson, pp. 161-180.

Billings, S.E., Kattenhorn, S.A., 2005. The great thickness debate: Ice shell thickness models for Europa and comparisons with estimates based on flexure at ridges. Icarus 177, 397-412.

Collins, G.C., Head, J.W., Pappalardo, R.T., Spaun, N.A., 2000. Evaluation of models for the formation of chaotic terrain on Europa. J. Geophys. Res. 105, 1709-1716.

Coulter, C.E., Kattenhorn, S.A., Schenk, P.M., 2009. Topographic profile analysis and morphologic characterization of Europa's double ridges. Lunar Planet. Sci. XL, 1960 (abstract).

Coulter, C.E., Kattenhorn, S.A., 2010. The morphology of Europa's ridges examined in a detailed topographic and kinematic survey. Eos (Fall Suppl.) 91, P21B-1599.

Crisp, J., 1984. Rates of magma emplacement and volcanic output. J. Volcanology and Geothermal Res. 20, 177-211.

Damptz, A.L., Dombard, A.J., 2011. Time-dependent flexure of the lithospheres on the icy satellites of Jupiter and Saturn. Icarus 216, 86-88.

Dombard, A.J., McKinnon, W.B., 2000. Long-term retention of impact crater topography on Ganymede. Geophys. Res. Lett. 27, 3663-3666.

Dombard, A.J., McKinnon, W.B., 2006a. Elastoviscoplastic relaxation of impact crater topography with application to Ganymede and Callisto. J. Geophys. Res. 111, E01001, doi:10.1029/2005JE002445.

Dombard, A.J., McKinnon, W.B., 2006b. Folding of Europa's icy lithosphere: an analysis of viscous-plastic buckling and subsequent topographic relaxation. J. Struct. Geol. 28, 2259-2269.

Dombard, A.J., Patterson, G.W., Prockter, L.M., 2007. Sill injection on icy satellites inferred from ridge-induced flexure on Europa. Eos (Fall Suppl.) 88, P21B-0549.

Gaidos, E.J., Nimmo, F., 2000. Tectonics and water on Europa. Nature 405, 637.

Gammon, P.H., Kiefte, H., Clouter, M.J., 1983. Elastic constraints of ice samples by Brillouin spectroscopy. J. Phys. Chem. 87, 4025-4029.

Goldsby, D.L., Kohlstedt, D.L., 2001. Superplastic deformation of ice: Experimental observations. J. Geophys. Res. 106, 11,017-11,030.

Greeley, R., Chyba, C., Head, J.W., McCord, T., McKinnon, W.B., Pappalardo, R.T., 2004. Geology of Europa. In: Bagenal, F., Dowling, T., McKinnon. W. (Eds.), Jupiter: The Planet, Satellites and Magnetosphere, Cambridge Univ. Press, Cambridge, pp. 329-362.

Greenberg, R., Geissler, P.E., Hoppa, G., Tufts, B.R., Durda, D.D., Pappalardo, R., Head, J.W., Greeley, R., Sullivan, R., Carr, M.H., 1998. Tectonic processes on Europa: Tidal stresses, mechanical response, and visible features. Icarus 135, 64-78.

Han, L., Melosh, H.J., 2010. Origin of Europa's ridges by incremental ice-wedging. Eos (Fall Suppl.) 91, P33B-1577.

Han, L., Showman, A.P., 2008. Implications of shear heating and fracture zones for ridge formation on Europa. Geophys. Res. Lett. 35, L03202, doi:10.1029/2007GL031957.

Head, J.W., Pappalardo, R.T., Sullivan, R., 1999. Europa: Morphogical characteristics of ridges and triple bands from Galileo data (E4 and E6) and assessment of a linear diapirism model. J. Geophys. Res. 104, 24,223-24,236.

Hurford, T.A., Beyer, R.A., Schmidt, B., Preblich, B., Sarid, A.R., Greenberg, R., 2005. Flexure of Europa's lithosphere due to ridge-loading. Icarus 177, 380-396.

Hussmann, H., Spohn, T., 2004. Thermal-orbital evolution of Io and Europa. Icarus 171, 391-410.

Kadel, S.D., Fagents, S.A., Greeley, R., Galileo SSI Team, 1998. Trough-bounding ridge pairs on Europa: Considerations for an endogenic model of formation. Lunar Planet. Sci. XXIX, 1078 (abstract).

Kattenhorn, S., Hurford, T., 2009. Tectonics of Europa. In: Pappalardo, R.T., McKinnon, W.B., Khurana, K. (Eds.), Europa, The University of Arizona Press, Tucson, AZ, pp. 199-236.

Kay, J.P., Dombard, A.J., 2011. Unstable deformation and the formation of the equatorial bulge of Iapetus. Lunar Planet. Sci. XLII, 2441 (abstract).

Kirk, R.L., Stevenson, D.J., 1987. Thermal evolution of a differentiated Ganymede and implications for surface features. Icarus 69, 91-134.

Kivelson, M.G., Khurana, K.K., Russell, C.T., Volwerk, M., Walker, R.J., Zimmer, C., 2000. Galileo magnetometer measurements: A stronger case for a subsurface ocean at Europa. Science 289, 1340-1343.

Kleinhans, M.G., Markies, H., de Vet, S.J., in 't Veld, A.C., Postema, F.N., 2011. Static and dynamic angles of repose in loose granular materials under reduced gravity. J. Geophys. Res. 116, E11004, doi:10.1029/2011JE003865.

Klinger, J., 1980. Influence of phase transition of ice on the heat and mass balance of comets. Science 209, 271-272.

Manga, M., Wang, C.-Y., 2007. Pressurized oceans and the eruption of liquid water on Europa and Enceladus. Geophys. Res. Lett. 34, L07201, doi:10.1029/2007GL029297.

Melosh, H.J., Turtle, E.P., 2004. Ridges on Europa: Origin by incremental ice-wedging. Lunar Planet. Sci. XXXV, 2029 (abstract).

Moore, J.M., Black, G., Buratti, B., Phillips, C.B., Spencer, J., Sullivan, R., 2009. Surface properties, regolith, and landscape degradation. In: Pappalardo, R.T., McKinnon, W.B., Khurana, K.K. (Eds.), Europa, Univ. of Arizona Press, Tucson, pp. 329-349.

Nimmo, F., Gaidos. E.J., 2002. Strike-slip motion and double ridge formation on Europa. J. Geophys. Res. 107, doi:10.1029/2000JE001476.

Nimmo, F., Spencer, J.R., Pappalardo, R.T., Mullen, M.E., 2007. Shear heating as the origin of the plumes and heat flux on Enceladus. Nature 447, 289-291.

O'Brien, D.P., Geissler, P., Greenberg, R., 2002. A melt-through model for chaos formation on Europa. Icarus 156, 152-161.

Pappalardo, R.T., Coon, M.D., 1996. A sea ice analog for the surface of Europa. Lunar Planet. Sci. XXVIII, 997-998 (abstract).

Pappalardo, R.T., et al., 1999. Does Europa have a subsurface ocean? Evaluation of the geological evidence. J Geophys. Res. 104, 24,015-24,056.

Petrenko, V.F., Whitworth, R.W., 1999. Physics of Ice. Oxford University Press.

Prockter, L.M., Patterson, G.W., 2009. Morphology and evolution of Europa's ridges and bands. In: Pappalardo, R.T., McKinnon, W.B., Khurana, K.K. (Eds.), Europa, Univ. of Arizona Press, Tucson, pp. 237-258.

Ruiz, J., 2005. The heat flow of Europa. Icarus 177, 438-446.

Schenk, P.M., 2009. Slope characteristics of Europa: Constraints for landers and radar sounding. Geophys. Res. Lett. 36, L15204, doi:10.1029/2009GL039062.

Schenk, P.M., Turtle, E.P., 2009. Europa's impact craters: Probes of the icy shell. In: Pappalardo, R.T., McKinnon, W.B., Khurana, K.K. (Eds.), Europa, Univ. of Arizona Press, Tucson, pp. 181-198.

Schenk, P.M., Chapman, C.R., Zahnle, K., Moore, J.M., 2009. Ages and interiors: The cratering record of the Galilean satellites. In: Bagenal, F., Dowling, T., McKinnon. W. (Eds.), Jupiter: The Planet, Satellites and Magnetosphere, Cambridge Univ. Press, Cambridge, pp. 427-456.

Schubert, G., Anderson, J.D., Spohn, T., McKinnon, W.B., 2004. Interior composition, structure, and dynamics of the Galilean satellites. In: Bagenal, F., Dowling, T., McKinnon. W. (Eds.), Jupiter: The Planet, Satellites and Magnetosphere, Cambridge Univ. Press, Cambridge, pp. 281-306.

Schubert, G., Sohl, F., Hussmann, H., 2009. Interior of Europa. In: Pappalardo, R.T., McKinnon, W.B., Khurana, K.K. (Eds.), Europa, Univ. of Arizona Press, Tucson, pp. 353-368.

Sotin, C., Tobie, G., Wahr, J., McKinnon, W.B., 2009. Tides and tidal heating on Europa. In: Pappalardo, R.T., McKinnon, W.B., Khurana, K.K. (Eds.), Europa, Univ. of Arizona Press, Tucson, pp. 85-118.

Sullivan, R. et al., 1998. Episodic plate separation and fracture infill on the surface of Europa. Nature 391, 371-373.

Tufts, B.R., 1998. Lithospheric Displacement Features on Europa and their Interpretation, Ph.D. dissertation, Univ. of Arizona, Tucson.

Tufts, B.R., Greenberg, R., Hoppa, G., Geissler, P., 1999. Astypalaea Linea, a large-scale strike-slip fault on Europa. Icarus 141, 53-64.

Turcotte, D.L., Schubert, G., 2002. Geodynamics. Cambridge University Press, 2nd edition.

Turtle, E.P., Melosh, H.J., Phillips, C.B., 1998. Tectonic modeling of the formation of europan ridges. Eos (Fall Suppl.) 79, F541.

Zhou, Y.C., Xu, B.H., Yu, A.B., Zulli, P., 2002. An experimental and numerical study of the angle of repose of coarse spheres. Powder Tech. 125, 45-54.

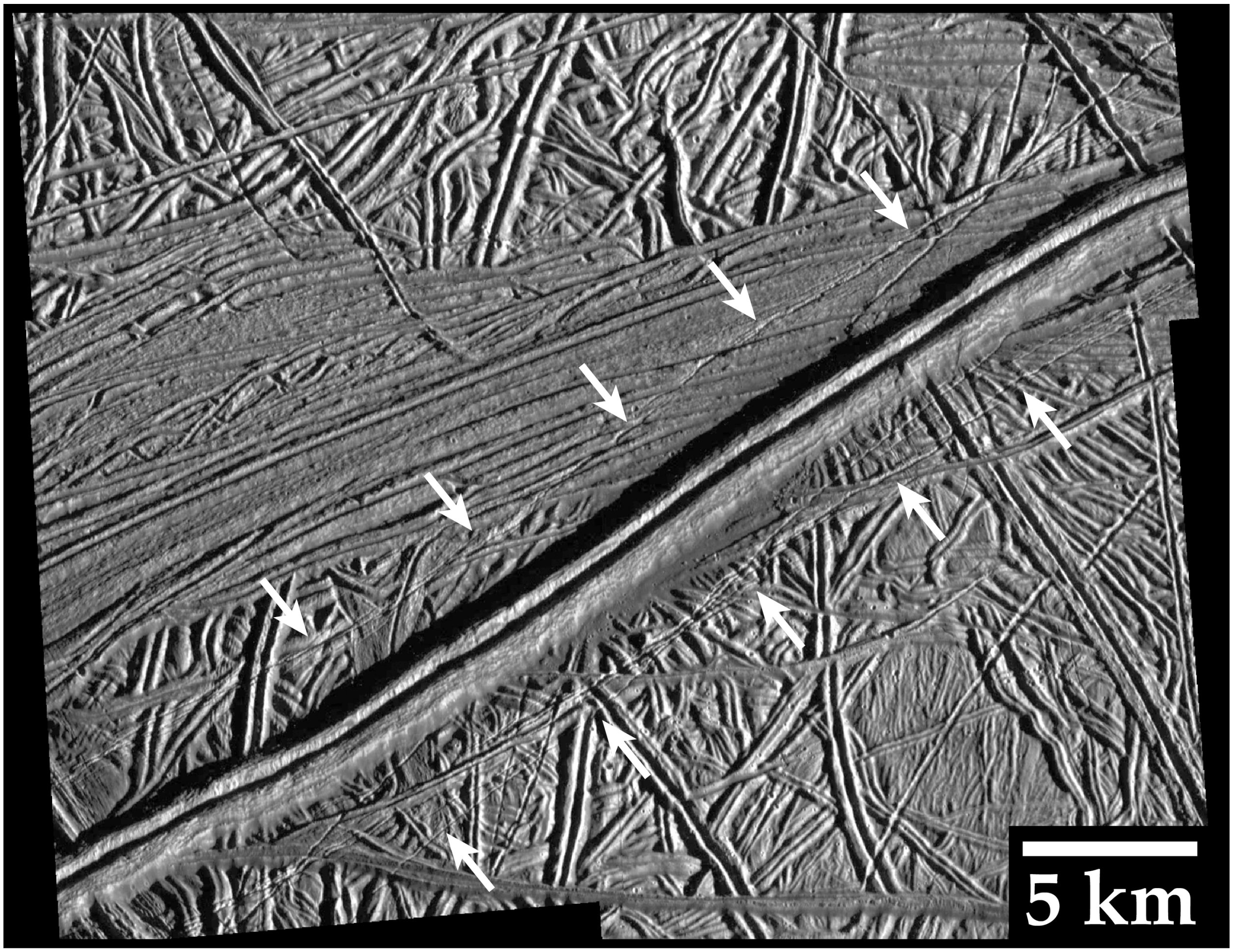

Figure 1. This high-resolution view of the Androgeos Linea double ridge (14.7 °N, 273.4 °W) was taken by NASA's Galileo spacecraft during its E6 orbit. It is obvious that Androgeos Linea is but the latest is a long history of double-ridge formation in this area. The arrows mark the flanking, subparallel cracks.

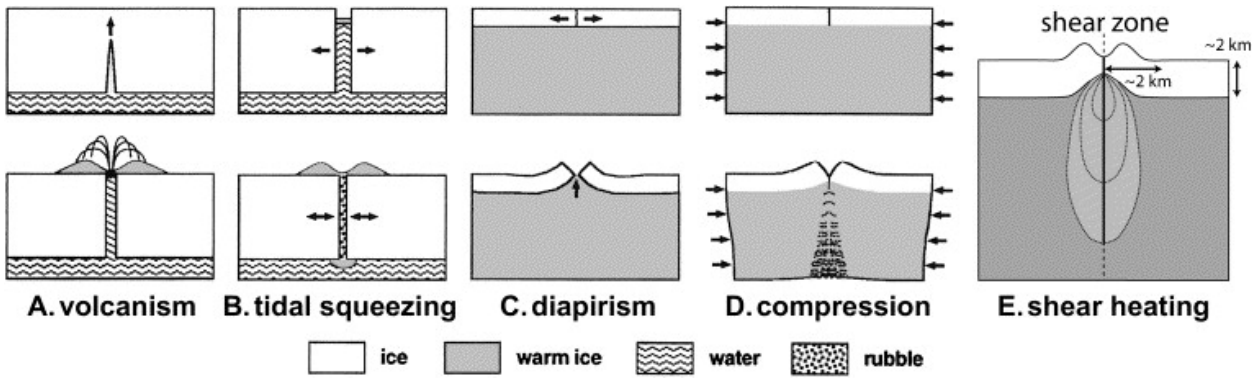

Figure 2. This figure schematically reviews various models for double-ridge formation on Europa. From Aydin (2006), which was adapted from Pappalardo et al. (1999) and Nimmo and Gaidos (2002).

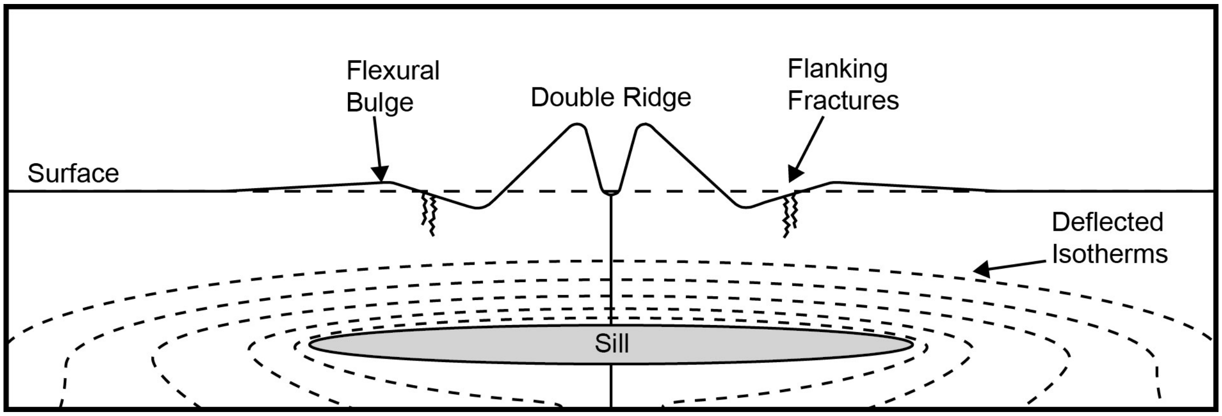

Figure 3. A cross-sectional schematic cartoon illustrating a model for a cryoclastically emplaced double ridge, underlain by a cryomagmatic sill. The presence of the sill may heat the overlying line, deflecting isotherms (dashed lines) upwards, locally thinning the lithosphere and thus possibly explaining the flexure seen at some double ridges.

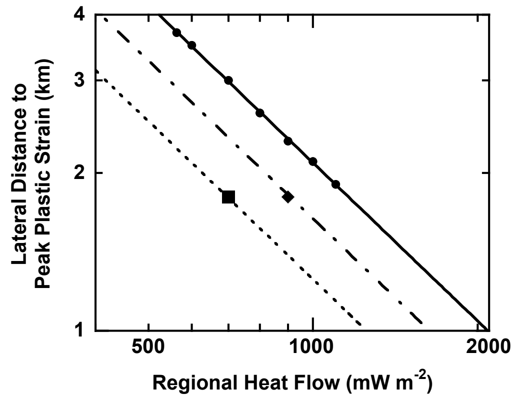

Figure 4. Lateral distance to peak plastic strain as a function of the background heat flow, for simulations without any thermal anomaly. The symbol size is coincident with the uncertainty, which is based off the mesh resolution of 100 m. The solid line is a fit to the cases with nominal parameters for Europa. The dash-dot line marks the situation of a higher surface temperature, while the dotted line marks the situation of a higher surface temperature and a smaller ice grain size. Io-like heat flows are needed to explain the flexure observed at double ridges, implicating a thermal anomaly in the creation of the flexure.

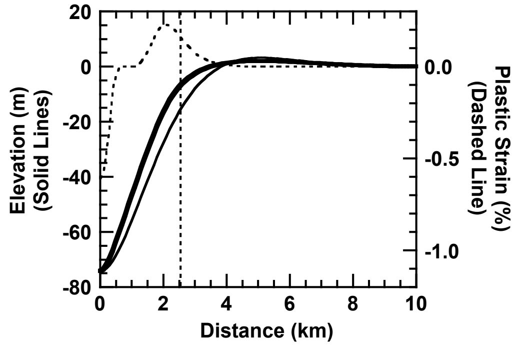

Figure 5. Elevation profiles (left axis, solid lines) and a plastic strain profile (right axis, dashed line) as a function distance away from the central axis. The thick solid line is the elevation profile from our simulation, while the thin solid line is from a model of a thin (~140 m) elastic plate subjected to a line load and with a flexural bulge cresting at the same distance as our simulation results (~5.1 km). The dashed vertical line marks the distance to maximum bending stresses (i.e., the site of peak plastic strain) in this elastic plate model; this distance is somewhat farther from the central axis than that to the peak plastic strain in our simulation.

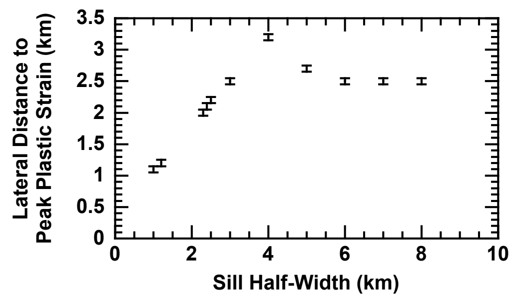

Figure 6. Lateral distance from the central axis to peak plastic strain as a function of sill half-width, for simulations testing the cryovolcanic sill model. The distance to peak plastic strain scales roughly with the sill width for narrow sills, but plateaus at distances well within the edge of the thermal anomaly for wide sills.

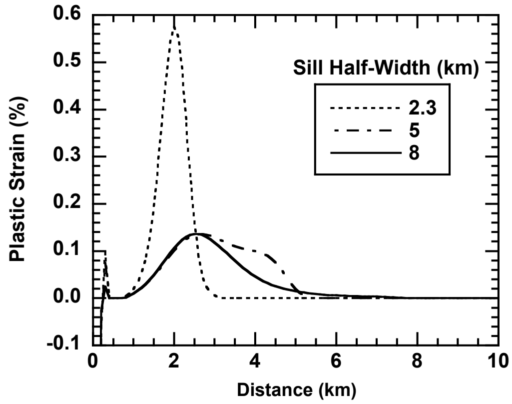

Figure 7. Profiles of lateral plastic strain as a function of surface distance away from the central axis, for simulations with sills of different widths. A zone of plastic strain over the thermal anomaly is seen for a case with a wide sill, with a peak in the plastic strain seen at distances well within the edge of the sill. On the other hand, plastic strains are strongly concentrated at the edge of the thermal anomaly for narrow sills. Sills of intermediate widths show transitional behavior.